Isotopic studies of Sn–Cr binary oxide catalysts for methane total oxidation

Yue-xiang Zhu [a,*], Irmina K. Murwani [b], Chang-jun Zhou [a], Erhard Kemnitz [b], and You-chang Xie [a]

[a] State Key Laboratory for Structural Chemistry of Unstable and Stable Species, College of Chemistry and Molecular Engineering, Peking University, 100871 Beijing, China

[b] Institute of Chemistry, Humboldt University, Brook Taylor Str. 2, D-12489 Berlin, Germany

Received 29 August 2002; accepted 1 November 2002

A series of Sn–Cr binary oxide catalysts were prepared by a co-current co-precipitation method and tested for methane total oxidation. The binary oxide catalysts have much higher surface areas and catalytic activities for methane oxidation than pure SnO_2. CrO_x/SnO_2 with a Cr/Sn atomic ratio of 3 : 7 displays the highest activity. Selected samples were subjected to temperature-programmed ^{18}O isotope-exchange measurements. Both complete and partial heteromolecular ^{18}O isotope exchange, as well as oxygen release, was observed for all catalysts. Reaction between CH_4 and $^{18}O_2$ under static conditions was performed to investigate the reaction mechanism and it was found that the total oxidation of methane over Sn–Cr binary oxide catalysts occurs via a redox cycle with the chromium ion in a high oxidation state as the active center. Oxygen mobility of the catalyst plays an important role in the total oxidation of methane, but too high a mobility leads to very high oxygen release and a reduction of the surface reoxidability. This causes a decrease in the catalytic oxidation activity.

KEY WORDS: ^{18}O isotope exchange; Sn–Cr binary oxide; methane total oxidation.

1. Introduction

Catalytic total oxidation of methane is an effective way to use methane as an energy source, or prevent it from polluting the atmosphere [1]. Supported precious metals are the most commonly used catalysts for this reaction [2–6]. However, due to the limited source and high price of precious metals, much effort has been focused on base metal oxides such as cobalt-containing oxides, manganese oxides, and perovskites [7–11]. Recently, Wang and Xie reported that Sn–Cr solid solution catalysts prepared by the reaction of $SnCl_2$ and K_2CrO_4 solutions showed novel thermal stability and quite high activity for methane total oxidation. They attributed the catalytic property to the enlarged surface area and the formation of more active oxygen species [12,13].

It is generally accepted that the catalytic activity and selectivity is largely governed by the nature of the surface oxygen species involved in oxidation catalysis on metal oxides [14–19]. High mobility of the oxygen species on the catalyst is essential for the oxidation property. Lattice oxygen sites essentially lead to selective oxidation, whereas both lattice oxygen and adsorbed oxygen species participate in deep oxidation. Oxygen isotope exchange is a common method to study the uptake/release properties of oxygen and the participation of oxygen from the catalyst in oxidation reactions [20–27]. The isotopic tracer method is very effective in the study of reaction mechanisms [27–29].

In this paper, Sn–Cr binary oxide catalysts prepared by a co-current co-precipitation method [30] were investigated using the temperature-programmed ^{18}O isotope-exchange method. The relationship between oxygen mobility and methane total oxidation activity is discussed. The $^{18}O_2$ and CH_4 reaction was also performed to study the reaction mechanism.

2. Experimental

2.1. Catalyst preparation

The co-current co-precipitation method described previously [30] was used to prepare SnO_2 and Sn–Cr binary oxide samples. $SnCl_4$ and/or $Cr(NO_3)_3$ aqueous solutions were added simultaneously with 1 N NaOH solutions to a certain amount of NH_4HCO_3 solution, keeping a pH of 7–8. Afterwards, the precipitate was filtered and washed with NH_4HCO_3 solution and distilled water until the filtrate was free of Cl^- ions as tested with 0.5 M $AgNO_3$. The product was then dried at 110 °C followed by calcination at 600 °C in air for 4 h.

2.2. Catalyst characterization

The BET specific surface areas were measured using a Micromeritics ASAP 2010 analyzer with nitrogen as the adsorbate. X-ray powder diffraction (XRD) patterns were recorded using a Rigaku D/MAX-2000 with Ni-filtered CuKα radiation at 40 kV and 100 mA. X-ray

* To whom correspondence should be addressed.

1011-372X/03/0200-0205/0

photoelectron spectroscopy (XPS) analysis of Cr2p and O1s peaks was carried out using a VG-ESCA-LAB-5 photoelectron spectrometer using AlKα radiation.

2.3. Catalytic tests

Catalytic activity measurements were carried out at atmospheric pressure in a fixed-bed flow micro-reactor. The catalyst powder was pressed to pellets and then crushed and sieved to 60–80 mesh. The volume composition of the feed gas was 1.0% CH_4 in air and the space velocity of the feed gas was 20 000/h. A K-type thermocouple was placed in the middle of the catalyst bed to monitor the reaction temperature. The reactants and products were analyzed with an on-line SQ-206 gas chromatograph equipped with a hydrogen flame ionization detector and a methanator of nickel catalyst to convert CO_2 and CO to CH_4. A 4 m long Porapak Q column was employed to separate CH_4, CO, and CO_2. The peaks of CH_4, CO, and CO_2 were processed by a computer and the conversion of methane was calculated automatically. It should be noted that during the measurement no CO was detected.

2.4. ^{18}O isotopic exchange

The temperature-programmed $^{18}O_2$ isotope-exchange measurements were carried out in a quartz reactor with an on-line-coupled quadruple mass spectrometer (QMG421 I, Pfeiffer Vacuum GmbH). The detailed experimental set-up is described in an earlier publication [22]. Before starting the measurement, each sample (about 300 mg) was heated at 400 °C for 4 h in an air flow ($p = 200$ Pa) in order to remove H_2O, CO_2, and other molecules from the surface of the oxide. After cooling to 100 °C, a gas mixture of Ar, $^{16}O_2$, and $^{18}O_2$ with a pressure ratio of 6:1:1 and a total pressure of 120 Pa was introduced into the reaction system. All measurements were performed in the temperature range 100–700 °C with a heating rate of 10 °C/min. Between the gas phase $^{16}O_2$ and $^{18}O_2$ and the metal oxide several processes such as oxygen uptake/release, homomolecular gas phase ^{18}O isotope exchange, partial heteromolecular ^{18}O isotope exchange, and complete heteromolecular ^{18}O isotope exchange may take place separately or simultaneously depending on the nature of the compound and/or the temperature range investigated [31,32]. The temperature dependence of the ionic currents (IC) of $^{16}O_2$, $^{18}O_2$, and $^{16}O^{18}O$ of the gas phase provides information on the occurrence of the above mentioned processes. In order to differentiate between simultaneous processes, four different coefficients are derived from the measured ionic currents. The definitions of the four coefficients have been comprehensively elucidated and applied in earlier publications [20–25]; they will only be shortly summarized as follows.

(1) The coefficient s represents the oxygen partial pressure of the gas phase standardized by the oxygen partial pressure at the beginning of the measurement. The coefficient s changes only when oxygen uptake/release occurs.

(2) The coefficient c expresses the proportion of ^{18}O relative to the total oxygen content in the gas phase. c decreases when oxygen is released, and partial or complete heteromolecular exchange processes take place.

(3) The coefficient y describes the deviation of the actual partial pressure from the equilibrium partial pressure of the mixed isotope $^{16}O^{18}O$. A decrease in y shows the occurrence of partial heteromolecular or homomolecular ^{18}O isotope exchange, while an increase in y indicates the release of $^{16}O_2$.

(4) The coefficient v represents the fraction of ^{18}O in the gas phase that originates from the $^{16}O^{18}O$ molecules. v increases when any of the three types of ^{18}O isotope exchange processes takes place.

2.5. CH_4 oxidation with $^{18}O_2$ under static conditions

The reaction between $^{18}O_2$ and CH_4 under static conditions was measured in a similar manner. After pretreatment, a gas mixture of CH_4, $^{18}O_2$, and Ar with a pressure ratio of 1:20:80 was introduced into the reaction system and the sample was heated to 700 °C with a heating rate of 10 °C/min. The onset temperature of the oxidation reaction and the oxidation product distribution were then measured.

3. Results and discussion

3.1. Total oxidation of methane over Sn–Cr binary oxide catalysts

The catalytic properties of Sn–Cr binary oxide catalysts with various compositions were tested. Their activities are presented as the temperatures of 10, 50, and 98% CH_4 conversion, T_{10}, T_{50}, and T_{98}, in table 1,

Table 1
Composition, BET surface areas, and catalytic properties of Sn–Cr binary oxide catalysts

Sample	Cr/Sn atomic ratio	S_{BET} (m^2/g)	T_{10} (°C)	T_{50} (°C)	T_{98} (°C)
SnO_2	–	29	390	466	540
SnCr1	1:9	111	300	410	520
SnCr2	2:8	131	320	406	510
SnCr3	3:7	133	320	400	490
SnCr4	4:6	107	<300	403	520
SnCr5	5:5	153	300	403	550
SnCr6	6:4	159	325	404	540
SnCr7	7:3	130	340	415	540
SnCr8	8:2	107	340	425	>550

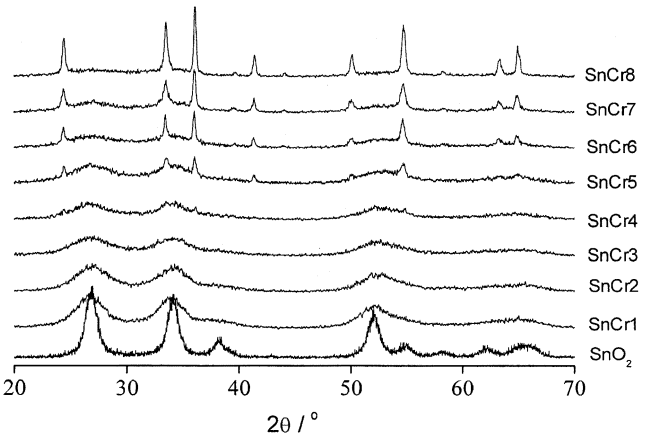

Figure 1. XRD patterns of SnO_2 and Sn–Cr binary oxide samples.

together with their compositions and BET surface areas. Pure SnO_2 is quite active for CH_4 total oxidation, the respective temperatures are 390, 466, and 540 °C. A small amount of chromium leads to a significant increase in the catalytic activity, especially at low temperatures. T_{10} decreases from 390 to 300–320 °C, and T_{50} and T_{98} also decrease with increasing chromium content. SnCr3 with a Cr/Sn atomic ratio of 3:7 exhibits the highest activity. For samples with higher chromium content, T_{10} and T_{50} are still lower than those of pure SnO_2, but T_{98} becomes comparable to or even higher than that of SnO_2.

The XRD patterns of Sn–Cr binary oxide catalysts prepared by the co-current co-precipitation method are shown in figure 1. Pure SnO_2 shows intensive and sharp peaks, revealing its high crystallinity. For the Sn–Cr binary oxide samples, the diffraction peaks of Cr_2O_3 begin to appear when the Cr/Sn atomic ratio exceeds 3:7 and increases with Cr content. In the patterns of samples with lower Cr content, only the diffraction peaks of SnO_2 are observed, but the peaks are much broader than those of pure oxide, indicating that the particle size is much smaller.

Comparing the XRD patterns with the results reported by Wang and Xie [13], it can be seen that for the Sn–Cr binary oxides prepared by reaction between $SnCl_2$ and K_2CrO_4 solutions, diffraction peaks of Cr_2O_3 begin to appear when the chromium content is increased to a Cr/Sn atomic ratio of 7:3. In comparison, peaks characteristic of Cr_2O_3 appear at much lower chromium content for the samples in figure 1. This is probably a result of the different materials used in the preparation. The redox reaction method [13] caused a higher extent of chromium doping into the SnO_2 lattice to form a solid solution, while the XRD characterization of the samples investigated in this paper did not show any proof of a solid solution and the chromium oxide may exist in a monolayer-dispersed state [33]. Actually, the existing state and position of the chromium ions in the sample are very complicated and closely related to the preparation method. However, the presence of chromium ions in higher oxidation states was determined by XPS analysis. The oxidation of Cr(III) to Cr(V) and Cr(VI) after calcination in air was confirmed in previous papers [34–37]. Solymosi *et al.* [37] reported that Cr^{3+} ions incorporated in the surface layer of SnO_2 were oxidized to higher oxidation states. A significant increase in activity for both the decomposition and the oxidation of $CHCl_3$ observed is due to the easy reduction and oxidation of chromium ions incorporated in the surface layer of SnO_2.

The specific surface areas of the samples are also listed in table 1. The surface area of pure SnO_2 is very low, about 30 m^2/g, whereas all of the Sn–Cr binary oxides display surface areas exceeding 100 m^2/g, which are much higher than the respective samples with the same composition reported previously [13]. This is in agreement with the results of XRD analysis and demonstrates that the Sn–Cr binary oxide catalysts prepared here are more resistant to thermal sintering than pure SnO_2. The dispersion of chromium oxide on the surface of SnO_2 hinders the sintering of tin oxide during calcination and thus markedly improves the thermal stability and surface area of the sample obtained [38]. Obviously, the high surface area is an important reason for the enhanced catalytic activity, but not the only one. SnCr5 and SnCr6 with higher specific surface areas than SnCr3 exhibit much lower activities for total conversion. As reported by Wang and Xie [13] and other authors [14–19], the properties of the oxygen species are also crucial to catalytic performance. This will be discussed in the following sections.

3.2. *Temperature-programmed ^{18}O isotope exchange*

Temperature-programmed ^{18}O isotope-exchange measurements of selected samples were carried out to investigate the oxygen species of these catalysts. The samples selected were SnCr3 with the highest activity for methane total oxidation, SnCr1 with lower chromium content than SnCr3, SnCr5 with higher chromium content, and the pure SnO_2.

The results of the ^{18}O isotope-exchange reaction of SnCr3 catalyst are illustrated in figure 2. Figure 2(a) shows the change in the ionic currents of $^{16}O_2$, $^{18}O_2$, and $^{16}O^{18}O$ with reaction temperature. In figure 2(b), the temperature dependence of the four coefficients is presented. In the temperature range 100–280 °C, all the ionic currents of $^{16}O_2$, $^{18}O_2$, and $^{16}O^{18}O$ as well as the four coefficients are constant. At about 280 °C, $^{18}O_2$ begins to decrease and continues to do so up to 700 °C. At the same time, the $^{16}O_2$ and $^{16}O^{18}O$ ionic currents and the coefficients s and v increase with temperature from 280 to 700 °C, while the coefficient c decreases. However, the rates of increase or decrease are different depending on the temperature range. The y coefficient first decreases with reaction temperature demonstrating

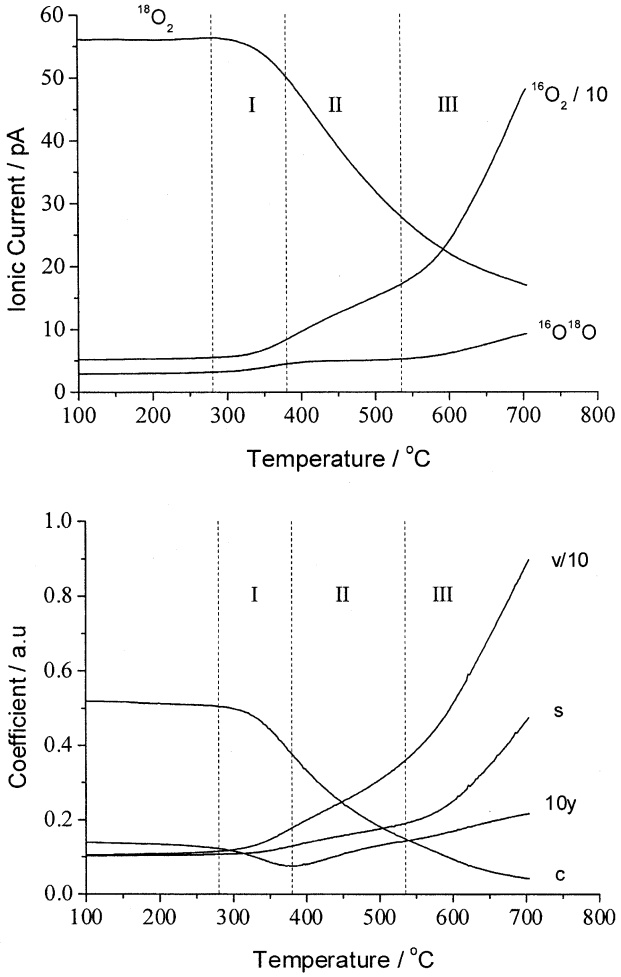

Figure 2. Ionic current curves of $^{18}O_2$, $^{16}O_2$, and $^{16}O^{18}O$ and variations of the coefficients for SnCr3.

partial heteromolecular isotope exchange, reaching a minimum at 380 °C, after which it increases up to 700 °C.

According to the variation of the ionic currents and the coefficients, the reaction process can be divided into three regions. The first region, between 280 and 380 °C, a decrease in $^{18}O_2$ ionic current is accompanied by increasing $^{16}O^{18}O$ and $^{16}O_2$ ionic currents. The *v* and *s* coefficients increase, while coefficients *c* and *y* decrease. From these results, it can be deduced that both partial heteromolecular isotope exchange (PHE) and oxygen release take place in this temperature range, PHE predominating over the oxygen release. In the second region, 380–535 °C, $^{18}O_2$ decreases rapidly, but $^{16}O^{18}O$ remains relatively constant, while $^{16}O_2$ increases at a higher rate than in the first region. The corresponding coefficients *v*, *s*, and *c* show variations similar to those in the first region, but *y* increases with reaction temperature. Complete heteromolecular isotope exchange (CHE) and oxygen release take place in this temperature range. In the third region, between 535 and 700 °C, $^{18}O_2$ continues to decrease with rapid increase in $^{16}O_2$ and $^{16}O^{18}O$. The coefficients *v* and *s* also increase at a much higher rate than in the first and second regions. The

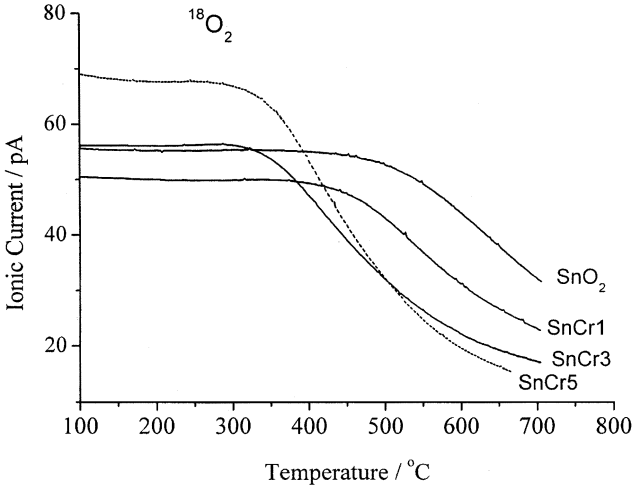

Figure 3. Ionic current curves of $^{18}O_2$ for different samples.

coefficient *y* also increases, and the decrease in coefficient *c* slows down. Therefore, PHE and oxygen release as predominant process take place at an increased rate in this temperature range. CHE occurs simultaneously.

Compared to SnCr3, samples SnCr5 and SnCr1 have more or less the same behavior in the isotope exchange reaction, except for different temperature regions. Pure SnO_2 exhibits much lower activity. Figures 3–6 compare the temperature dependence of ionic currents and coefficients for different samples. The processes taking place on each sample during temperature-programmed ^{18}O isotope exchange are summarized in table 2.

SnO_2 displays the highest onset temperature for ^{18}O isotope exchange and oxygen release. SnCr1, with small amounts of chromium, shows a lower onset temperature than SnO_2 implying an enhanced activity in the isotope exchange reaction. However, SnO_2 generates more $^{16}O^{18}O$ than SnCr1 above 550 °C, suggesting that PHE plays a more important role for SnO_2 than for SnCr1. Samples with higher chromium

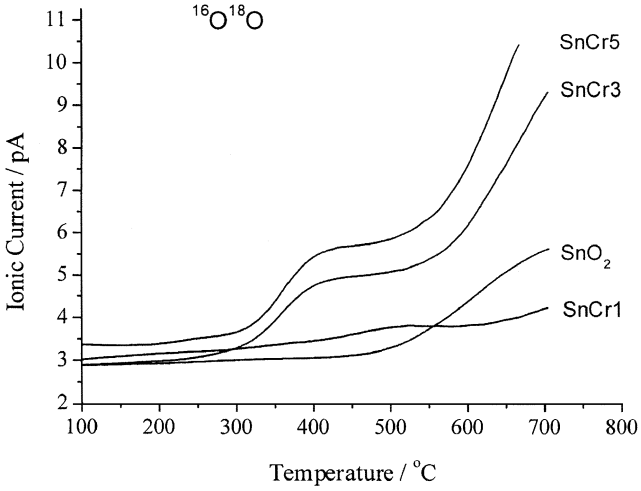

Figure 4. Ionic current curves of $^{16}O^{18}O$ for different samples.

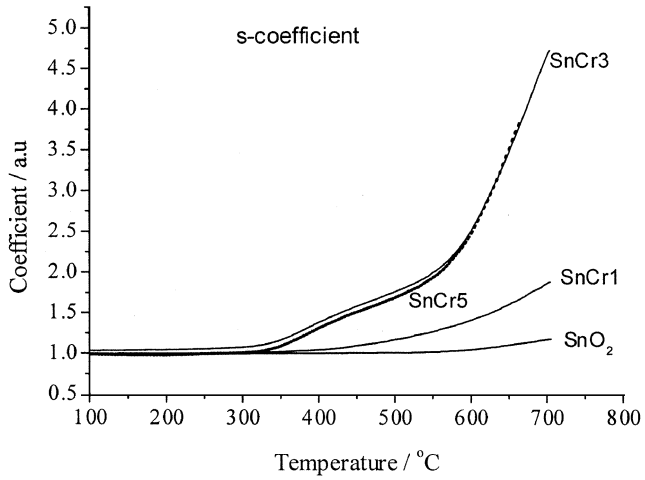

Figure 5. Variation of *s* coefficients for different samples.

content, SnCr3 and SnCr5, show very high and comparable activities in the isotope exchange reaction.

3.3. Reaction of $^{18}O_2$ and CH_4 under static conditions

In the previous section, the $^{18}O_2$ isotope exchange behavior of the samples was investigated. In order to understand and confirm the reaction mechanism, oxidation of methane with $^{18}O_2$ isotope was performed as described above using the same apparatus.

Figure 7 depicts the temperature dependence of the ionic currents of the reactant and the products over the most active SnCr3 catalyst. Consumption of CH_4 resulted in the formation of $C^{16}O_2$, with traces of $C^{16}O^{18}O$ and almost no $C^{18}O_2$. Considering the ratio of ^{18}O, which is the only oxygen source in the original gas phase, in the oxidation products, one can deduce that the oxidizing agent in the reaction is the metal in a high oxidation state, the oxygen being transferred into the gaseous products from the solid. Hence, a possible reaction pathway can be summarized as follows:

$$CH_{4(ad)} + 4\,{}^{16}O^{2-}_{(s)} \rightarrow C^{16}O_{2(g)} + 2H_2O_{(g)} + 8e^-$$

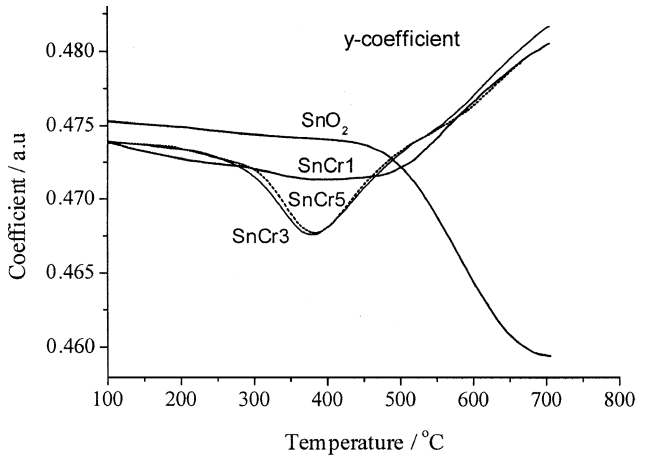

Figure 6. Variation of *y* coefficients for different samples.

Table 2
Temperature range of $^{18}O_2$ isotope exchange and oxygen release processes for the samples

Sample	Temperature range (°C)		
	PHE [a] and R [b]; PHE dominates over R	CHE [c] and R [b]	CHE [c], PHE [a], and R [b]; more PHE and R
SnO_2	400–440	–	440–700
SnCr1	340–400	400–590 [d]	590–700
SnCr3	280–380	380–535	535–700
SnCr5	300–385	385–515	515–700

[a] Partial heteromolecular isotope exchange.
[b] Oxygen release.
[c] Complete heteromolecular isotope exchange.
[d] PHE takes place here.

$$8/n\,Cr^{6+}_{(s)} + 8e^- \rightarrow 8/n\,Cr^{(6-n)+}_{(s)} \quad (n = 1, 2, 3)$$

$$8/n\,Cr^{(6-n)+}_{(s)} + 2\,{}^{18}O_2(g) \rightarrow 8/n\,Cr^{6+} + 4\,{}^{18}O^{2-}_{(s)}.$$

Of course, Cr(V) and Sn(IV) may also participate similarly in the reaction. Such a redox mechanism is normal for transition metal oxide catalysts [25]. As the oxygen in the products originates from the solid surface containing $^{16}O^{2-}$ only at the beginning, far more $C^{16}O_2$ is produced than $C^{16}O^{18}O$ and $C^{18}O_2$. With longer reaction times, more and more ^{18}O is incorporated into the solid via the above mentioned mechanism and complete heteromolecular isotope exchange. This leads to a gradual increase in the ionic current of $C^{16}O^{18}O$.

Figure 8 shows the formation of $C^{16}O_2$ and $C^{16}O^{18}O$ during the oxidation reaction over different samples. The catalytic activities observed here are consistent with the results obtained by flow reaction. The most active catalyst, SnCr3, also displays the highest activity in isotope exchange. Clearly, high mobility of oxygen species leads to high oxidative activity. However, SnCr5 shows a comparable activity in $^{18}O_2$ isotope exchange, but its activity for methane total oxidation is

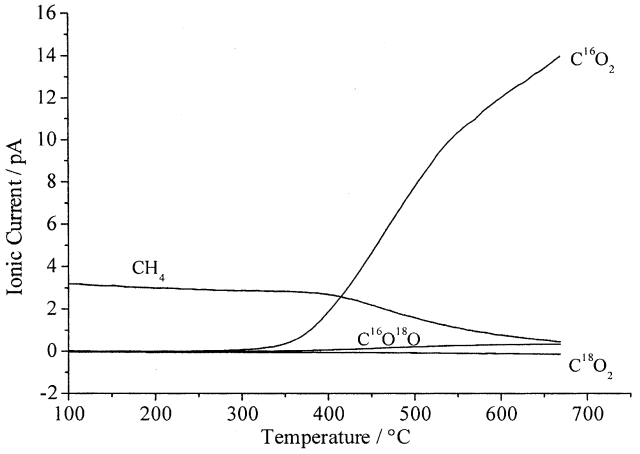

Figure 7. Ionic current curves of CH_4, $C^{16}O_2$, $C^{16}O^{18}O$, and $C^{18}O_2$ during CH_4 oxidation with $^{18}O_2$ on SnCr3.

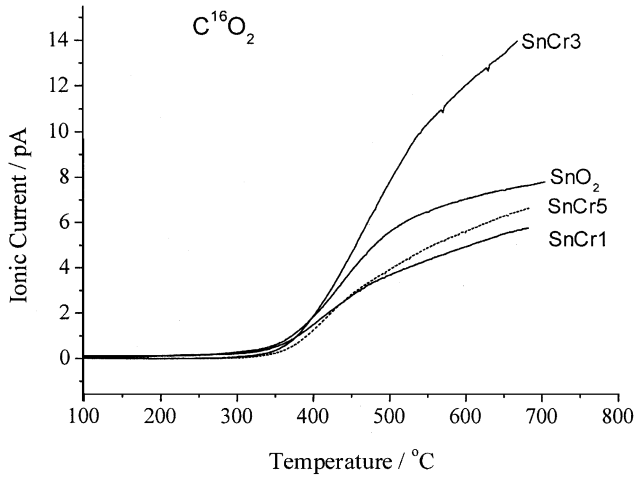

(a)

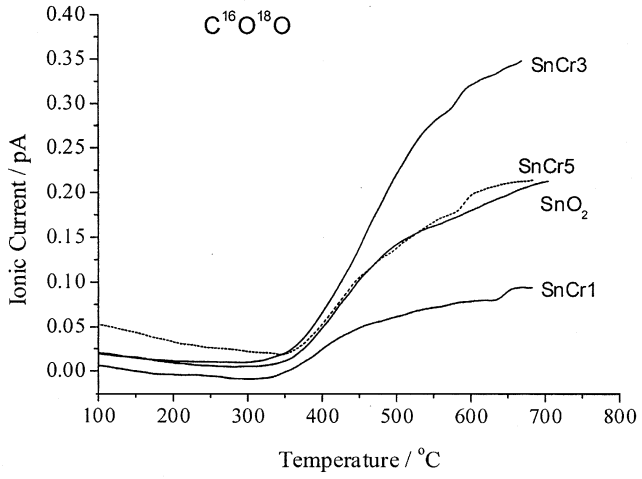

(b)

Figure 8. Comparison of the ionic curves of (a) $C^{16}O_2$ and (b) $C^{16}O^{18}O$ during CH_4 oxidation with $^{18}O_2$ on different samples.

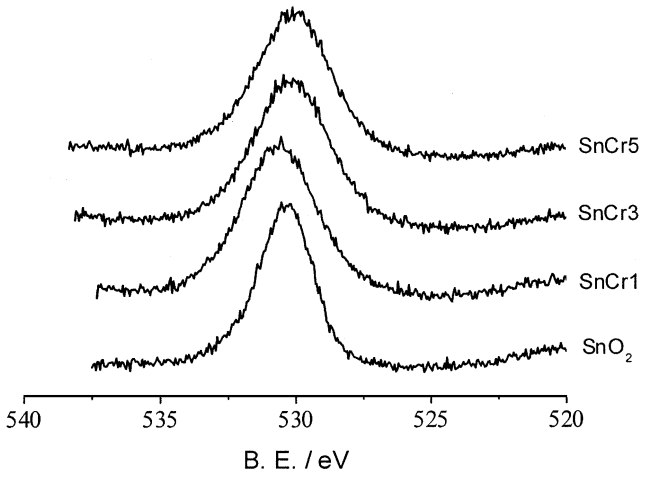

Figure 9. O1s peaks of different samples.

lower than that of SnCr3. Comparing the *s* and $^{16}O_2$ curves of SnCr3 and SnCr5, it can be seen that SnCr5 exhibits a higher rate of increase for *s* and $^{16}O_2$ above 533 °C than SnCr3, implying a weaker bonding of surface oxygen in SnCr5. XPS characterization also proves this point. As shown in figure 9, the O1s peak of SnO_2 is a narrow one centered at 530.3 eV, while the O1s peaks of Sn–Cr binary oxide samples are much broader indicating the generation of more than one type of oxygen species. The average binding energies of O1s for SnCr1, SnCr3, and SnCr5 are 530.5, 530.1, and 530.0 eV respectively, demonstrating a permanent decrease in the bonding energy of the oxygen to the solid with increasing chromium content. These are closely related to the activity in the isotope exchange reactions. It is generally considered that complete oxidation catalysts have considerable amounts of weakly bound oxygen on the surface, and the weaker the oxygen bonding with the catalyst surface the more efficient is complete oxidation with this catalyst [14,15]. However, very weakly bound oxygen leads to very high oxygen release and a reduction of the surface re-oxidability. This causes a decrease in the catalytic oxidation activity [39].

It is also interesting to note that SnO_2 generates more $C^{16}O_2$ (figure 8(a)) but comparable or less $C^{16}O^{18}O$ than SnCr5 (figure 8(b)). This result can be attributed to the higher isotope exchange activity of SnCr5.

4. Conclusion

Sn–Cr binary oxide catalysts prepared by co-current co-precipitation show much higher surface areas and catalytic activities for methane oxidation than pure SnO_2. SnCr3 with a Cr/Sn atomic ratio of 3:7 displays the highest activity. Temperature-programmed ^{18}O isotope-exchange measurements show that both complete and partial heteromolecular ^{18}O isotope exchange as well as oxygen release take place for all catalysts. Reaction between CH_4 and $^{18}O_2$ under static conditions reveals that the oxidation of methane over Sn–Cr binary oxide catalyst occurs via a redox cycle where the chromium ions in a high oxidation state are the active centers. Oxygen mobility of the catalyst is very important for the total oxidation of methane, but very high mobility leads to a decrease in the catalytic oxidation activity.

Acknowledgment

We gratefully acknowledge the financial support from the Major State Basic Research Development Program (Grant No. G2000077503), National Science Foundation of China (29803001), and Cooperation project between NSFC and DFG (20111130499).

References

[1] M.M. Zwinkel, S.G. Jaras and P.C. Menon, Catal. Rev. Sci. Eng. 35 (1993) 319.
[2] P. Reyes, A. Figueroa, G.G. Pecchi and J.L. Fierro, Catal. Today 62 (2000) 209.
[3] C. Bozo, N. Guilhaume and J. Herrmann, J. Catal. 203 (2001) 393.
[4] E. Marceau, H. Lauron-Pernot and M. Che, J. Catal. 197 (2001) 394.
[5] D. Ciuparu and L. Pfefferle, Appl. Catal. A 218 (2001) 197.
[6] R. Spinicci and A. Tofanari, Appl. Catal. A 227 (2002) 159.
[7] A.Q.M. Boon, H.M. Huisman and J.W. Geus, J. Mol. Catal. 75 (1992) 293.
[8] X. Wang and Y.C. Xie, Catal. Lett. 72 (2001) 51.
[9] S.F. Ji, T.C. Xiao, H.T. Wang, E. Flahaut, K.S. Coleman and M.L.H. Green, Catal. Lett. 75 (2001) 65.
[10] I. Rosso, E. Garrone, F. Geobaldo, B. Onida, G. Saracco and V. Specchia, Appl. Catal. B: Environ. 34 (2001) 29.
[11] S. Cimino, R. Pirone and L. Lisi, Appl. Catal. B: Environ. 35 (2002) 243.
[12] X. Wang and Y.C. Xie, Chem. Lett. 3 (2001) 216.
[13] X. Wang and Y.C. Xie, Appl. Catal. B: Environ. 35 (2001) 85.
[14] V.D. Sokolovskii, Catal. Rev. Sci. Eng. 32 (1990) 1.
[15] H. Kung and M. Kung, Adv. Catal. 33 (1984) 159.
[16] M.I. Zaki, M.A. Hasan, L. Pasupulety and K. Kumari, New J. Chem. (1998) 875.
[17] Z. Zhong, Q. Yan, X. Fu and J. Gong, Chem. Commun. (1996) 1745.
[18] K. Omata, O. Yamazaki, K. Tomita and K. Fujimoto, J. Chem. Soc. Chem. Commun. (1994) 1637.
[19] W. Ding, Y. Chen and X. Fu, Catal. Lett. 23 (1994) 69.
[20] G.K. Boreskov, Adv. Catal. 15 (1964) 285.
[21] V.S. Muzikantov, G.I. Panov and G.K. Boreskov, Kinet. Katal. 14 (1973) 948.
[22] E. Kemnitz, D.H. Menz, C. Stoecker and T. Olesch, Thermochim. Acta 225 (1993) 119.
[23] E. Kemnitz, A.A. Galkin, T. Olesch, S. Scheurell, A.P. Mozhaev and G.N. Mazo, J. Therm. Anal. 48 (1997) 997.
[24] I.A. Koudriashov, G.N. Mazo, I.K. Murwani, S. Scheurell and E. Kemnitz, J. Therm. Anal. Cal. 63 (2001) 59.
[25] I.K. Murwani, S. Scheurell, M. Feist and E. Kemnitz, J. Therm. Anal. Cal. 69 (2002) 9.
[26] M.K. Dongare, V. Ramaswamy, C.S. Gopinath, A.V. Ramaswamy, S. Scheurell, M. Brueckner and E. Kemnitz, J. Catal. 199 (2001) 209.
[27] A. Holmgren, D. Duprez and B. Andersson, J. Catal. 182 (1999) 441.
[28] Au-Yeung, K. Chen, A.T. Bell and E. Iglesia, J. Catal. 188 (1999) 132.
[29] J.C. Li, C. Yu and S. Shen, Catal. Lett. 75 (2001) 183.
[30] J. Ma, Y.X. Zhu, J.Y. Wei, X.H. Cai and Y.C. Xie, Stud. Surf. Sci. Catal. 130 (2000) 617.
[31] C. Doornkamp, M. Clement and V. Ponec, J. Catal. 182 (1999) 390.
[32] C. Doornkamp, M. Clement, X. Gao, G. Deo, I.E. Wachs and V. Ponec, J. Catal. 185 (1999) 415.
[33] Y.C. Xie and Y.Q. Tang, Adv. Catal. 37 (1990) 1.
[34] P.G. Harrison, N.C. Lloyd and W. Daniell, J. Phys. Chem. B 102 (1998) 10627.
[35] S.A. Best, R.G. Squires and R.A. Walton, J. Catal. 47 (1977) 299.
[36] S.D. Yim, K.H. Chang, D.J. Koh, I.S. Nam and Y.G. Kim, Catal. Today 63 (2000) 215.
[37] F. Solymosi, J. Rasko, E. Papp, A. Oszko and T. Bansagi, Appl. Catal. A 131 (1995) 55.
[38] B.Y. Zhao, X.P. Xu, H.R. Ma and D.H. Sun, Catal. Lett. 45 (1997) 237.
[39] N. Yamazoe and Y. Teraoka, Catal. Today 8 (1990) 175.